Compressive Sensing for RADARSAT-2 Tomography

David Kirkland
Defence Research and Development Canada - Ottawa Research Centre

***Abstract*—Satellite Synthetic Aperture Radar (SAR) systems can achieve vertical resolution by using multiple platform passes to create a synthetic aperture in the elevation direction. Often the distribution of the orbits is not optimal for traditional forms of tomographic processing. Due to the random nature of the orbit positions and the relatively small number of measurements, a compressive sensing (CS) approach for achieving vertical resolution is utilized to determine the likely achievable performance of RADARSAT-2 (R2) in tomographic operation.**

I. Introduction

Multi-pass Interferometric Synthetic Aperture Radar (In-SAR) systems utilize coherent data collections from multiple passes to provide an estimate of the terrain elevation at each range-azimuth pixel in the SAR image. The inherent assumption in interferometric processing is that only one dominant scatter exists within each range-azimuth pixel. SAR Tomographic techniques provide elevation resolution within the range-azimuth pixel so the vertical structure can be resolved. In the multi-pass geometry a vertical synthetic aperture can be created to provide elevation discrimination in much the same way that conventional SAR systems use a synthetic aperture to achieve azimuth resolution.

The creation of a vertical synthetic aperture differs for the typical SAR configuration in two major aspects. First, the number of samples used to synthesize vertical aperture is typically quite small in comparison to the creation of an azimuth synthetic aperture. Second, the acquisition positions of the satellite platform are not uniformly sampled in the spatial domain. These conditions make it difficult to apply traditional Fourier based focusing techniques. Instead, specialized procedures to deal with the ill-conditioned problem need to used. Some of the techniques which have been applied to both the multi-baseline In-SAR and tomographic problems include the truncated SVD [1], [2] and non-linear least squares (NLS) [2] approaches. More recently compressive sensing [3] approaches have been applied [4]–[7]. In this paper, orbital information from RADARSAT-2 is used to measure the capability to resolve two targets in a range/azimuth pixel utilizing a compressive sensing approach under various signal to noise ratios.

II. Signal Model

Consider the satellite the multi-pass satellite SAR geometry shown in Fig. 1. The satellite sensor passes through N different orbits. The u axis is taken perpendicular to the line of sight. The position of each satellite pass is given by S_n, $n = 1, \ldots, N$. The projection of each satellite position onto the u axis is given by u_n, $n = 1, \ldots, N$. and $r_n = S_n - u_n$.The length of the perpendicular baseline $L_\perp$ is given by $|u_N - u_1|$. Any scatterers located along the s axis, denoted as s_m, will appear in the same range-azimuth cell of the SAR image. Fig 1 shows four discrete point are along the s axis as an example i.e., $m = 1, \ldots 4$. The range between the radar and the ground/elevation point s is given by

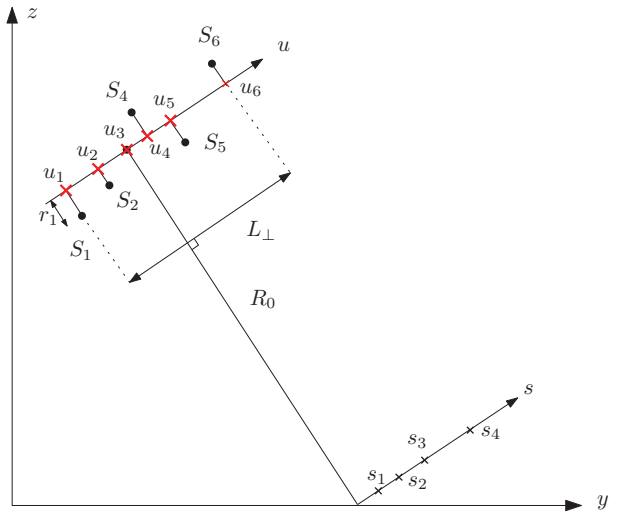

Figure 1. Multi-pass satellite tomographic SAR geometry. Black dots denote true satellite positions Red x's denote projection of satellite position onto u axis. Case for $N = 6$, $m = 4$.

$$R(u) = \sqrt{(R_0 + r_n)^2 + (u - s)^2},$$

in which R_0 is the slant range from the centre of the array to the ground. Since u and s will be small in comparison to R_0, the previous expression can be approximated by

$$\begin{aligned} R(u) &= \sqrt{(R_0 + r_n)^2 + u^2}\sqrt{1 - \frac{2us - s^2}{(R_0 + r_n)^2 + u^2}} \\ &\approx \sqrt{(R_0 + r_n)^2 + u^2} - \frac{us}{R_0} \end{aligned} \tag{1}$$

The corresponding two-way phase delay associated with this range is

$$\begin{aligned} \phi(u) &= -\frac{4\pi}{\lambda}\left[\sqrt{(R_0 + r_n)^2 + u^2} - \frac{us}{R_0}\right] \\ &= -2k\left[\sqrt{(R_0 + r_n)^2 + u^2} - \frac{us}{R_0}\right], \end{aligned} \tag{2}$$

where λ is the radar operating wavelength and $k = 2\pi/\lambda$ is the corresponding wave number. We denote the reference range as $R_{ref}(u) = \sqrt{(R_0 + r_n)^2 + u^2}$. The phase difference between the return signal of the radar and the reference range is given by

$$\begin{aligned} \triangle\phi(u) &= -2k\left[\sqrt{(R_0 + r_n)^2 + u^2} - \frac{us}{R_0}\right] \\ &\quad + 2k\sqrt{(R_0 + r_n)^2 + u^2} \\ &= 2k\frac{us}{R_0} \end{aligned} \tag{3}$$

This process of removing the phase associated with a fixed target reference point across the synthetic aperture is commonly used in Spotlight SAR signal processing and is often referred to as deramping [8].

Let g_n denote the signal in a fixed azimuth and range pixel at the nth satellite pass after removal of the phase due to the reference range. Then g_n consists of contributions from scatterers located along the s axis and is given by

$$g_n = \int \gamma(s) e^{j2ku_n s/R_0} ds \tag{4}$$

where $\gamma(s)$ represents the scattering strength along the s axis. The received signal for all the satellite passes can be written in vector format by letting $\mathbf{g} = [g_1, g_2, \ldots, g_N]^T$. By sampling at points s_m $(m = 1, \ldots M)$ along the s axis we can form a discrete model of the received signal given by

$$\begin{aligned} \mathbf{g} &= [\mathbf{a}(s_1), \mathbf{a}(s_2), \ldots, \mathbf{a}(s_M)]\boldsymbol{\gamma} \\ &= \mathbf{A}\boldsymbol{\gamma}, \end{aligned} \tag{5}$$

where

$$\boldsymbol{\gamma} = [\gamma(s_1), \gamma(s_2), \ldots, \gamma(s_M)]^T,$$

$$\mathbf{a}(s_m) = \left[e^{j2k\frac{u_1 s_m}{R_0}}, e^{j2k\frac{u_2 s_m}{R_0}}, \ldots, e^{j2k\frac{u_N s_m}{R_0}}\right]^T, \tag{6}$$

and u_n denotes the position of the nth satellite along the u axis as shown in Fig. 1. Note that in Fig. 1 $M = 4$ but it is typically much higher in practice.

The tomographic problem is to determine $\boldsymbol{\gamma}$, the vector of scattering coefficients, from the measurement vector $\mathbf{g}$. The standard approach is the least squares solution where the estimate of the true $\boldsymbol{\gamma}$ is given by

$$\hat{\boldsymbol{\gamma}} = \arg\min_{\boldsymbol{\gamma}} \|\mathbf{A}\boldsymbol{\gamma} - \mathbf{g}\|_2^2, \tag{7}$$

where $\hat{\boldsymbol{\gamma}}$ denotes the estimate. When $N < M$, the problem is under-determined, so no unique solution exists and the minimum norm solution is often uninformative. The compressive sensing approach is to regularize the problem through the use of the ℓ_1 norm on the solution vector. The ℓ_1 norm promotes sparsity in the solution vector so that only a few dominant components exist [9], [10]. Now the estimate is given by the solution to the following

$$\hat{\boldsymbol{\gamma}} = \arg\min_{\boldsymbol{\gamma}} \lambda \|\boldsymbol{\gamma}\|_1 + \|\mathbf{A}\boldsymbol{\gamma} - \mathbf{g}\|_2^2, \tag{8}$$

Parameter	Value
Wavelength	0.055 m
Range Resolution	3 m
Nominal Orbit Altitude	798 km

Table I
RADARSAT-2 PARAMETERS

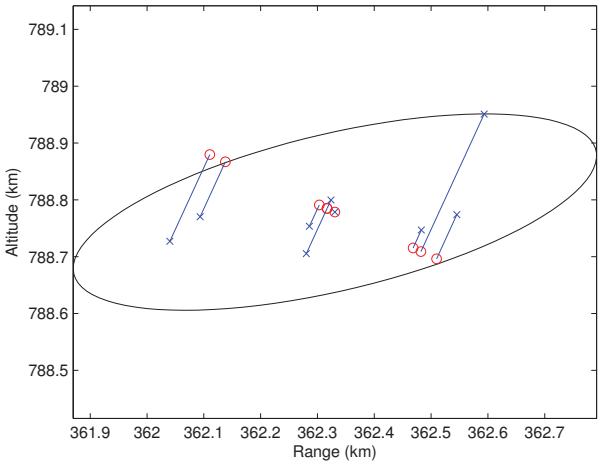

Figure 2. RADARSAT-2 Satellite simulation geometry for 8 orbits. Elevation $= 65.32°$. Perpendicular aperture 439 m.

where λ is a pre-selected weighting factor that provides a trade-off between the sparsity of the solution vector and fitting the data model. The optimization problem posed in (8) is convex and a number of algorithms have been developed to solve this problem. The Fast Iterative Shrinkage Thresholding Algorithm (FISTA) algorithm is used to generate the results in this paper [11].

III. Simulation Results

For the simulations, the historical ephemeris data for RADARSAT-2 was used. Eight coherent satellite passes over the the area of Ottawa, Canada are used to create the synthetic aperture. Note that for RADARSAT-2 coherent passes occur every 24 days. The first pass takes place on June 17, 2013. The mean elevation angle is $65.32°$ and the mean distance to the satellite is 868 km. Figure 2 illustrates the variation of the satellite geometries over the eight passes. The blue x's show the actual satellite position, while the the red circles indicate the projection of these positions onto the perpendicular baseline. In this geometry the size of the perpendicular baseline is 439 m. Principal Component Analysis (PCA) of the distribution of satellite passes is used to generate the ellipse and illustrate the variance of the orbital passes in the range and altitude directions. Table I lists the main operational parameters for RADARSAT-2.

The CS approach is used to determine to solve for the elevation estimates of a range/azimuth pixel containing two targets. In order to determine the effective resolution of the CS approach one target is kept at a constant elevation of 0 meters, while the second target starts at an elevation of 80 meters and is then decreased in 1.9 meters steps. The

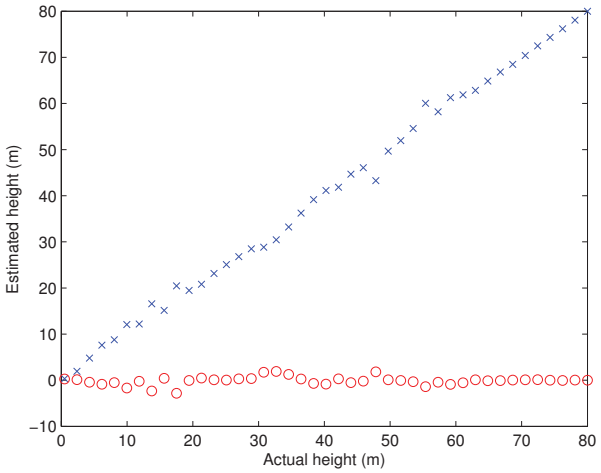

Figure 3. Estimated elevation positions, SNR=20 dB. Red o's denote estimated positions of the target at 0m elevation. Blue x's denote the estimated position of the second target.

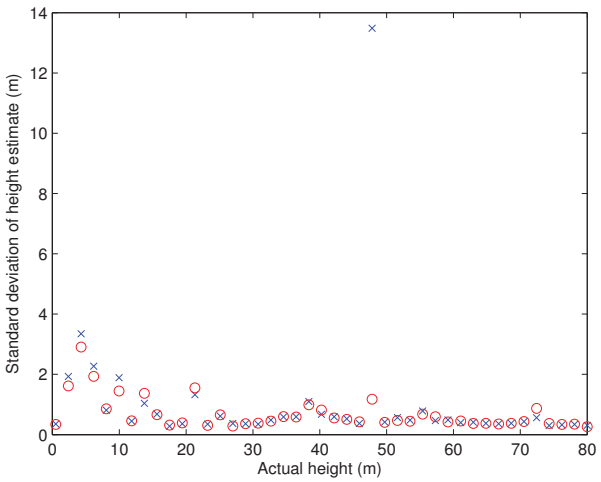

Figure 4. Standard deviation of the elevation estimates, SNR=20 dB. Red o's denote standard deviation of the target elevation estimates for the target at 0m elevation. Blue x's denote standard deviation of the second target's elevation estimates.

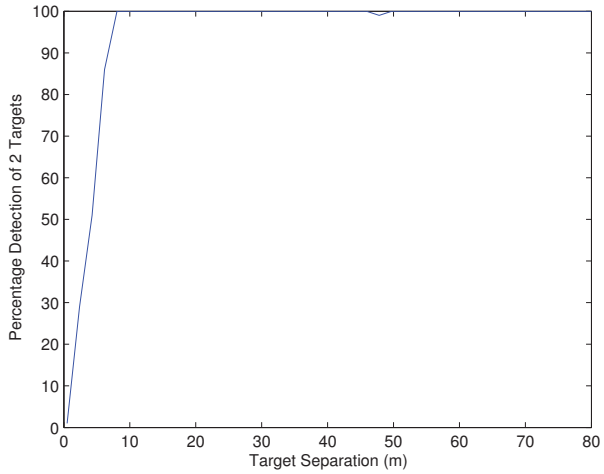

Figure 5. Probability of detection of 2 distinct targets. SNR=20dB.

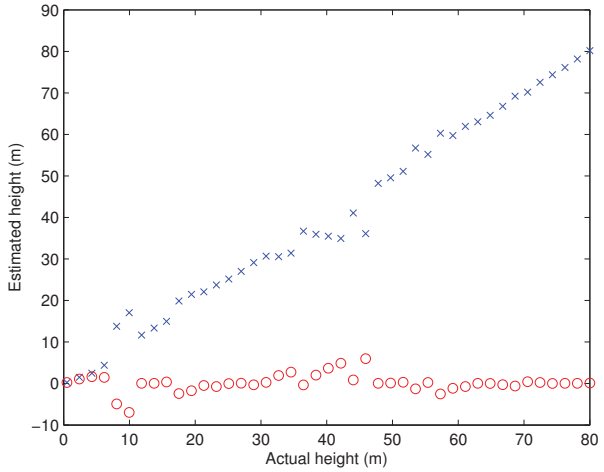

Figure 6. Estimated elevation positions, SNR=10 dB. Red o's denote estimated positions of the target at 0m elevation. Blue x's denote the estimated position of the second target.

sensing matrix consists of vectors corresponding to elevations uniformly separated by 0.55 meters, so there is an induced modeling error. This type of error is likely to occur in practice since the true elevations will not be know a priori. For each elevation position of the target 100 trials are conducted.

Figure 3 illustrates the mean of the estimated positions as a function of the second target's elevation when the SNR for each target is 20 dB. Examination of Figure 3 reveals that the mean estimates are consistent with the true elevations of the targets, although there is some deviation from the true value even when the targets are well separated. Figure 4 shows the standard deviation of the estimates as a function of the true height of the second target. In general the spread of the estimated elevations is less than than 1 m and the deviation tends to increase as the two targets get closer in elevation.

In some cases when the targets are closely positioned there is only a single detected target in the solution vector and this peak is assigned as the estimate for both targets. This can actually cause the error deviation to decrease. Even at this relatively high SNR there are spurious peaks in the error deviation of the target even though the targets are well separated e.g. 22m and 48m. Figure 5 illustrates the probability of detection of two distinct targets as a function of the elevation separation of the two targets. When both targets are assigned to the same elevation position in the solution vector this is treated as an error.

Figure 6 shows the mean of the estimated positions as a function of the second target's elevation, when the SNR for each target is 10 dB. Again, the mean estimate of the target elevations are mostly consistent with the true elevations, however there do appear to be a few elevations where the estimate is slightly biased. Figure 7 shows the standard deviation of the estimates as a function of the true height of the second target. Due to the decreased SNR the deviation of

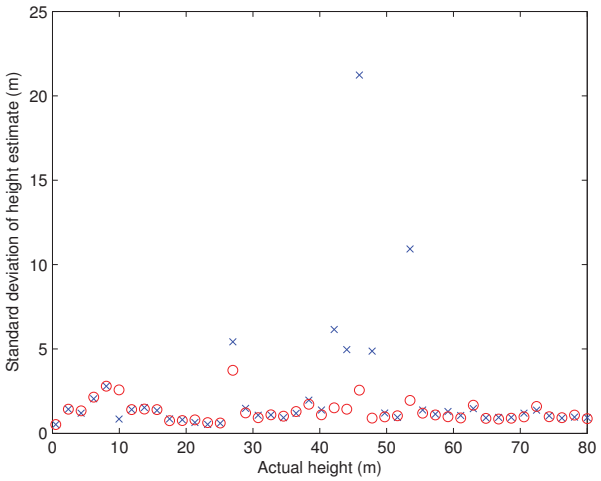

Figure 7. Standard deviation of the elevation estimates, SNR=10 dB. Red o's denote standard deviation of the target elevation estimates for the target at 0m elevation. Blue x's denote standard deviation of the second target's elevation estimates.

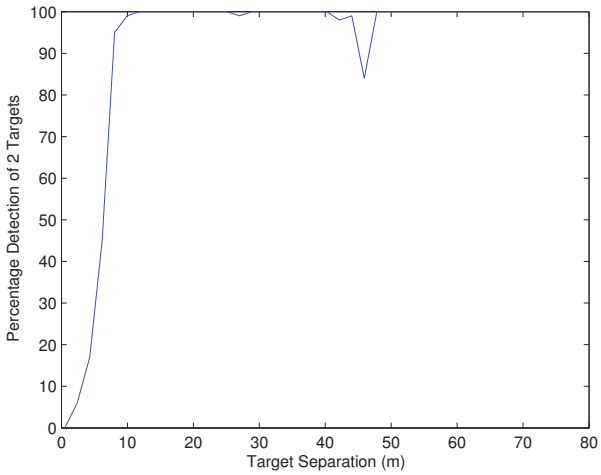

Figure 8. Probability of detection of 2 distinct targets. SNR=10dB.

the estimates has increased from the 20 dB SNR scenario and there are more elevations at which spuriously high deviations occur e.g. in the 40-50 m elevation range. Figure 8 depicts the probability of detection of 2 distinct targets when the SNR=10 dB. Comparison of Figure 8 and Figure 5 reveals that as the SNR decreases the target elevation separation distance increases to 8m to achieve a 95% detection rate. Figure 8 also reveals that even at large elevation separation distances the detection rate can experience large fluctuations e.g. when the target separation is 48m.

Figure 9 shows the mean of the estimated positions as a function of the second target's elevation, when the SNR for each target is 5 dB. Figure 10 shows the standard deviation of the estimates as a function of the true height of the second target. Figure 11 depicts the probability of detection of 2 distinct targets when the SNR is 5dB. At this SNR the detection rate displays wide fluctuations over the target

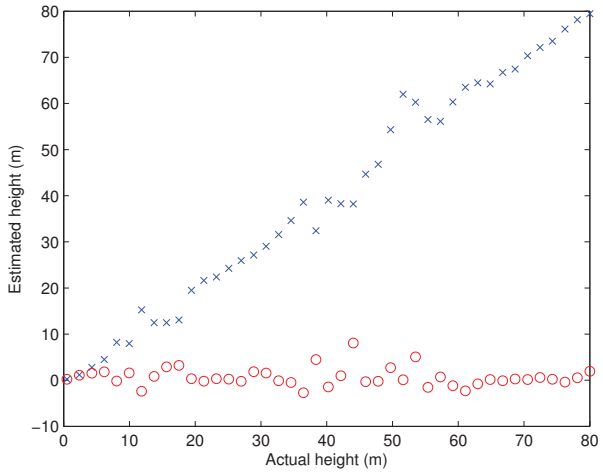

Figure 9. Estimated elevation positions, SNR=5 dB. Red o's denote estimated positions of the target at 0m elevation. Blue x's denote the estimated position of the second target.

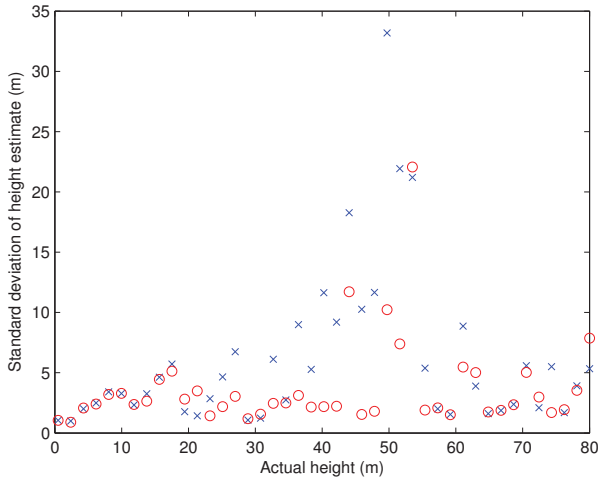

Figure 10. Standard deviation of the elevation estimates, SNR=5 dB. Red o's denote standard deviation of the target elevation estimates for the target at 0m elevation. Blue x's denote standard deviation of the second target's elevation estimates.

separation distances from 10 - 60m.

IV. Conclusions

The use of compressive sensing techniques can provide elevation resolution for tomographic processing of RADARSAT-2. The compressive sensing approach implicitly assumes the presence of a small number of targets in the range/azimuth cell under evaluation. The method works well for strong persistent targets, but further investigation is required to address decorrelation effects due to temporal/atmospheric variations and satellite position errors. With the compressive sensing approach many additional factors need to be investigated for practical tomographic operation e.g. the choice of the number and spacing of the vectors $\mathbf{a}(s_m)$ and the determination of the λ parameter on a pixel by pixel basis.

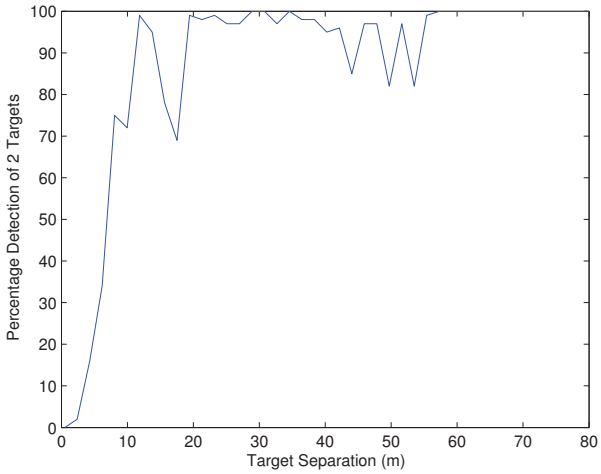

Figure 11. Probability of detection of 2 distinct targets. SNR=5dB.

REFERENCES

[1] G. Fornaro, F. Serafino, and F. Soldovieri, "Three-dimensional focusing with multipass sar data," *IEEE Transactions on Geoscience and Remote Sensing*, vol. 41, pp. 507–517, Mar. 2003.

[2] X. X. Zhu, *Spectral Estimation for Synthetic Aperture Radar Tomography*. Masters, Technische Universität München, Earth Oriented Space Science and Technology – ESPACE, Sept. 2008.

[3] E. Candes, J. Romberg, and T. Tao, "Robust uncertainty principles: exact signal reconstruction from highly incomplete frequency information," *Information Theory, IEEE Transactions on*, vol. 52, no. 2, pp. 489–509, 2006.

[4] A. Budillon, A. Evangelista, and G. Schirinzi, "Sar tomography from sparse samples," in *Geoscience and Remote Sensing Symposium,2009 IEEE International,IGARSS 2009*, vol. 4, pp. IV–865–IV–868, July 2009.

[5] A. Budillon, A. Evangelista, and G. Schirinzi, "Three-dimensional sar focusing from multipass signals using compressive sampling," *IEEE Transactions on Geoscience and Remote Sensing*, vol. 49, pp. 488–499, Jan. 2011.

[6] X. X. Zhu and R. Bamler, "Sparse reconstrcution techniques for sar tomography," in *2011 17th International Conference on Digital Signal Processing (DSP)*, pp. 1–8, 2011.

[7] X. X. Zhu and R. Bamler, "Tomographic sar inversion by l_1-norm regularization - the compressive sensing approach," *IEEE Transactions on Geoscience and Remote Sensing*, vol. 48, pp. 3839–3846, Oct. 2010.

[8] M. Soumekh, *Synthetic Aperture Radar Signal Processing with MATLAB Algorithms*. New York: Wiley-Interscience, 1 edition ed., Apr. 1999.

[9] E. J. Candès, J. K. Romberg, and T. Tao, "Stable signal recovery from incomplete and inaccurate measurements," *Communications on Pure and Applied Mathematics*, vol. 59, pp. 1207–1223, Aug. 2006.

[10] R. Baraniuk, "Compressive sensing," *IEEE Signal Processing Magazine*, vol. 24, pp. 118–121, July 2007.

[11] A. Beck and M. Teboulle, "A fast iterative shrinkage-thresholding algorithm for linear inverse problems," *SIAM Journal on Imaging Sciences*, vol. 2, no. 1, p. 183, 2009.